Comparison of several robust observers for automotive damper force estimation

Thanh-Phong Pham, Olivier Sename, Luc Dugard

Comparison of several robust observers for automotive damper force estimation

Thanh-Phong Pham[1,*], *Olivier* Sename[1,**], and *Luc* Dugard[1,***]

[1]Univ. Grenoble Alpes, CNRS, Grenoble INP[⊤], GIPSA-lab, 38000 Grenoble, France. [⊤]Institute of Engineering Univ. Grenoble Alpes

Abstract. This paper aims at comparing three robust observers used to estimate the damping force of of electrorheological (ER) damper in a vehicle suspension system. Firstly, a nonlinear quarter-car model, augmented with a first-order dynamical nonlinear damper model, is developed. The first two methods are designed considering the nonlinearity as an unknown input and minimizing the effect of the unknown input disturbances (including nonlinearity term, measurment noise, unknown road profile) on the estimation errors, by using an H_2 and H_∞ criterion, respectively. The latter method is to only minimize the effects of measurement noises and road profiles on the state variable estimation errors by using a H_∞ criterion while the nonlinearity is bounded through a Lipschitz condition. Two low-cost sensors signals (two accelerometers data from the sprung mass and the unsprung mass) are considered as inputs for the observer designs. Finally, the observers are implemented on the INOVE testbench from GIPSA-lab (1/5-scaled real vehicle) to assess and compare experimentally the performances of the approaches. Both simulations and experimental results demonstrate a better effectiveness of the latter observer in terms of the ability of estimating the damper force in real-time despite the nonlinearity, the measurement noises and the road disturbances.

1 Introduction

Now, in order to improve comfort and safety (road holding) for on-board passengers, semi-active suspensions are widespread in automotive applications because of their advantages compared to active and passive suspensions, see [1]. Study on control algorithms for automotive semi-active suspension system has received a lot of consideration. Some control strategies consider the damper force as the control input of the suspension system, and then use an inverse model or look-up tables for implementation (see [2, 3]). Others use the force tracking control schemes for local controller in order to attain control objectives (see [4]). Therefore, the real-time estimation of the damper force plays a vital role for the control and diagnosis of suspension systems since damper force sensors are difficult to install and expensive setups. To fulfill the demand, several estimation methodologies were proposed to estimate the damper force (see [5–10]). The key challenges to design damper force estimation are to reduce the cost of the required sensors, to take the dynamic behavior of damper into account, and to deal with the nonlinearity in presence of unknown road disturbance and sensor noises.

This paper presents a comparative study of three robust methodologies for solving the above challenges in designing the damper force observer of the semi-active suspension systems. The aspects of comparison are a) dealing with nonlinearity, b) minimizing the effect of sensor noise and unknown road profile to estimation errors. Note that such a comparison is proposed here for the first time in the case of suspension system. All of the observers use only two accelerometers in order to estimate the damper force in the quarter-car vehicle equipped with ER suspension. The designs of the observers are based on a nonlinear suspension model consisting of a quarter-car vehicle model, augmented with a first order dynamical nonlinear damper model. To deal with nonlinearity in the damper model, the two first observers ($\mathcal{H}_2$ and $\mathcal{H}_\infty$ observers) consider the nonlinearity as a unknown disturbance and use $\mathcal{H}_2$ and $\mathcal{H}_\infty$ norm to minimize the effect of three unknown input disturbances (nonlinearity, sensor noises, unknown road profile) on the estimation errors of state variables, respectively. In the latter observer ($\mathcal{H}_\infty$ Lipschitz observer), the nonlinearity is bounded by a Lipschitz condition, while the $\mathcal{H}_\infty$ norm is utilized to minimize only the effect of sensor noises and road profile disturbance on the estimation errors. To assess and compare experimentally the performances of the observers, they have been implemented on a real scaled-vehicle test bench, through the Matlab/Simulink real-time workshop.

The remainder of this paper is organized as follows:

- Section 2: Semi-active suspension modeling.
- Section 3: Observer designs.
- Section 4: Analysis and comparison of the observer designs: frequency and time domain simulations
- Section 5: Experimental validation and comparison
- Section 6: Conclusion

*e-mail: thanh-phong.pham2@gipsa-lab.grenoble-inp.fr
**e-mail: olivier.sename@gipsa-lab.grenoble-inp.fr
***e-mail: luc.dugard@gipsa-lab.grenoble-inp.fr

2 Semi-active suspension modeling and quarter-car system description

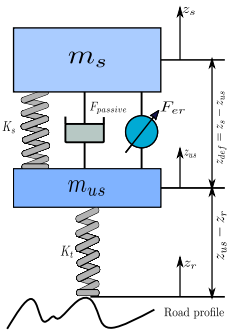

Figure 1. 1/4 car model with semi-active suspension

This section introduces the quarter-car model with the semi-active ER suspension system depicted in Fig.1. The quarter-car model equipped with the semi-active ER suspension system, depicted in Fig.1, is described in this section. The well-known model consists of the sprung mass (m_s), the unsprung mass (m_{us}), the suspension components located between (m_s) and (m_{us}) and the tire which is modelled as a spring with stiffness k_t. From second law of Newton for motion, the vertical system dynamics around the equilibrium are given as:

$$\begin{cases} m_s\ddot{z}_s &= -F_s - F_d \\ m_{us}\ddot{z}_{us} &= F_s + F_d - F_t \end{cases} \tag{1}$$

where $F_s = k_s(z_s - z_{us})$ is the spring force; $F_t = k_t(z_{us} - z_r)$ is the tire force; the damper force F_d is given as follows:

$$\begin{cases} F_d &= k_0(z_s - z_{us}) + c_0(\dot{z}_s - \dot{z}_{us}) + F_{er} \\ \dot{F}_{er} &= -\frac{1}{\tau}F_{er} + \frac{f_c}{\tau}\cdot u \cdot tanh(k_1(z_s - z_{us}) \\ & \quad +c_1(\dot{z}_s - \dot{z}_{us})) \end{cases} \tag{2}$$

where, $c_0, c_1, k_0, k_1, f_c, \tau$ are constant parameters; z_s and z_{us} are the displacements of the sprung and unsprung masses, respectively, z_r is the road displacement input.

By selecting the system states as $x = [x_1, x_2, x_3, x_4, x_5]^T = [z_s - z_{us}, \dot{z}_s, z_{us} - z_r, \dot{z}_{us}, F_{er}]^T \in \mathbb{R}^5$, the variables to be estimated $z = [x_1, x_2, x_4, x_5]^T \in \mathbb{R}^4$, the measured variables $y = [\ddot{z}_s, \ddot{z}_{us}]^T \in \mathbb{R}^2$ and the control input $u \in \mathbb{R}$, the system dynamics in the state-space representation can be written as follows

$$\begin{cases} \dot{x} &= Ax + B\Phi(x)\cdot u + D_1\omega \\ y &= Cx + D_2\omega \\ z &= C_z x \end{cases} \tag{3}$$

where

$$A = \begin{bmatrix} 0 & 1 & 0 & -1 & 0 \\ -\frac{(k_s+k_0)}{m_s} & -\frac{c_0}{m_s} & 0 & \frac{c_0}{m_s} & -\frac{1}{m_s} \\ 0 & 0 & 0 & 1 & 0 \\ \frac{(k_s+k_0)}{m_{us}} & \frac{c_0}{m_{us}} & -\frac{k_t}{m_{us}} & -\frac{c_0}{m_{us}} & \frac{1}{m_{us}} \\ 0 & 0 & 0 & 0 & -\frac{1}{\tau} \end{bmatrix}$$

$$C = \begin{bmatrix} -\frac{(k_s+k_0)}{m_s} & -\frac{c_0}{m_s} & 0 & \frac{c_0}{m_s} & -\frac{1}{m_s} \\ \frac{(k_s+k_0)}{m_{us}} & \frac{c_0}{m_{us}} & -\frac{k_t}{m_{us}} & -\frac{c_0}{m_{us}} & \frac{1}{m_{us}} \end{bmatrix}$$

$$B = \begin{bmatrix} 0 \\ 0 \\ 0 \\ 0 \\ \frac{f_c}{\tau} \end{bmatrix}, D_1 = \begin{bmatrix} 0 & 0 \\ 0 & 0 \\ -1 & 0 \\ 0 & 0 \\ 0 & 0 \end{bmatrix}, C_z = \begin{bmatrix} 1 & 0 & 0 & 0 & 0 & 0 \\ 0 & 1 & 0 & 0 & 0 & 0 \\ 0 & 0 & 0 & 1 & 0 & 0 \\ 0 & 0 & 0 & 0 & 0 & 1 \end{bmatrix}$$

$$D_2 = \begin{bmatrix} 0 & 0.01 \\ 0 & 0.01 \end{bmatrix}$$

$\omega = \begin{pmatrix} \dot{z}_r \\ n \end{pmatrix}$, in which, $\dot{z}_r$ is the road profile derivative and n represents the sensor noises.

Note that the measured outputs $y = [\ddot{z}_s, \ddot{z}_{us}]^T$ can be obtained easily from on board sensors (accelerometers).

3 Observer design

In this section, three observers (H_2, H_∞ and H_∞ Lipschitz observers) are developed to estimate the damping force accurately. In the designs, the sensor noises and road profile are considered as the unknown input ω. Therefore, H_2 and H_∞ observer are designed to minimize the effect of accounting for unknown disturbance ω and nonlinearity on the the state estimation errors while an H_∞ Lipschitz observer is proposed to only minimize the effect of the unknown input ω on the state estimation errors and to bound the nonlinearity by Lipschitz constant.

Firstly, H_2, H_∞ and H_∞ Lipschitz observers for the system (3) are defined in same form as follows:

$$\begin{cases} \dot{\hat{x}} = A\hat{x} + L(y - C\hat{x}) + B\Phi(\hat{x})\cdot u \\ \hat{z} = C_z\hat{x} \end{cases} \tag{4}$$

where $\hat{x}$ is the estimated states vector of x. $\hat{z}$ represents the estimated variables of the variables z. The observer gain L will be determined in the next steps The estimation error is given as

$$e(t) = x(t) - \hat{x}(t) \tag{5}$$

Differentiating $e(t)$ with respect to time and using (3) and (4), leads to:

$$\begin{cases} \dot{e} &= \dot{x} - \dot{\hat{x}} \\ &= (A - LC)e + B(\Phi(x) - \Phi(\hat{x}))\cdot u \\ &\quad +(D_1 - LD_2)\omega \\ e_z &= C_z e \end{cases} \tag{6}$$

Remark 1 In order to distinguish among three methodologies, the observer gain L is denoted as L_2 for the H_2 observer, L_∞ for the H_∞ observer and $L_{\infty L}$ for the H_∞ Lipschitz observer.

3.1 $\mathcal{H}_2$ observer design

As discussed previously, an $\mathcal{H}_2$ observer is designed to minimize the effect of ω and $(\Phi(x) - \Phi(\hat{x})) \cdot u$ on the state estimation errors e_F.

From (6) and Remark 3, one obtains

$$\begin{cases} \dot{e} &= (A - L_2C)e + D\omega_n \\ e_z &= C_z e \end{cases} \tag{7}$$

where $D = \begin{pmatrix} B & (D_1 - L_2D_2) \end{pmatrix}$, $\omega_n = \begin{pmatrix} (\Phi(x) - \Phi(\hat{x})) \cdot u \\ \omega \end{pmatrix}$

The transfer function between the state estimation error e_z and the unknown disturbance ω_n is:

$$T_{e_z\omega_n}(s) = C_z(sI - (A - L_2C))^{-1}D \tag{8}$$

The $\mathcal{H}_2$ observer design objectives are the following ones:

- The system (7) is stable for $\omega_n = 0$
- $\|T_{e_z\omega_n}(s)\|_2$ is minimized for $\omega_n \neq 0$

The following theorem solves the above problem into an LMI framework [11]

Theorem 1 Consider the system model (3) and the observer (4) . If there exist a symmetric positive definite matrix P_2 and a matrix Y_2 minimizing γ_2 such that:

$$\begin{bmatrix} P_2A + A^TP_2 - Y_2C - (Y_2C)^T & P_2B & P_2D_1 - Y_2D_2 \\ B^TP_2 & -I & 0 \\ D_1^TP_2 - (Y_2D_2)^T & 0 & -I \end{bmatrix} < 0$$
$$\begin{bmatrix} P_2 & C_z^T \\ C_z & \gamma_2 I \end{bmatrix} > 0 \tag{9}$$

then, the observer gain L_2 determined from $L_2 = P_2^{-1}Y_2$ ensures that the objectives are attained.

3.2 $\mathcal{H}_\infty$ observer design

Similarly to subsection 3.1, an $\mathcal{H}_\infty$ observer is designed to minimize the effect of ω and $(\Phi(x) - \Phi(\hat{x})) \cdot u$ on the state estimation errors e_z.

From (6) and Remark 3, one obtains

$$\begin{cases} \dot{e} &= (A - L_\infty C)e + D\omega_n \\ e_z &= C_z e \end{cases} \tag{10}$$

where $D = \begin{pmatrix} B & (D_1 - L_\infty D_2) \end{pmatrix}$, $\omega_n = \begin{pmatrix} \Phi(x) - \Phi(\hat{x}) \cdot u \\ \omega \end{pmatrix}$

The transfer function between the state estimation error e_z and the unknown disturbance ω_n is:

$$T_{e_z\omega_n}(s) = C_z(sI - (A - L_\infty C))^{-1}D \tag{11}$$

The $\mathcal{H}_\infty$ observer design objectives are the following ones:

- The system (10) is stable for $\omega_n = 0$
- $\|T_{e_z\omega_n}(s)\|_\infty$ is minimized for $\omega_n \neq 0$

The following theorem solves the above problem into an LMI framework [11]

Theorem 2 Consider the system model (3) and the observer (4). If there exist a symmetric positive definite matrix P_∞ and a matrix Y_∞ minimizing γ_∞ such that:

$$\begin{bmatrix} M & P_\infty B & P_\infty D_1 - Y_\infty D_2 \\ B^TP_\infty & -\gamma_\infty^2 I & 0 \\ D_1^TP_\infty - (Y_\infty D_2)^T & 0 & -\gamma_\infty^2 I \end{bmatrix} < 0 \tag{12}$$

where $M = P_\infty A + A^TP_\infty - Y_\infty C - (Y_\infty C)^T + C_z^TC_z$

then, the observer gain L_∞ determined from $L_\infty = P_\infty^{-1}Y_\infty$ ensures that the objectives are attained.

3.3 $\mathcal{H}_\infty$ Lipschitz observer design

In this section, the damping force is estimated through an $\mathcal{H}_\infty$ observer whose objectives are to minimize the effects of white noise and measurement noises on the estimation errors of the state variables and nonlinearity through a Lipschitz assumption.

Firstly, the control input function $\Phi(x)$ of the system (3) can be rewritten under the following form

$$\begin{aligned} \Phi(x) &= tanh(k_1x_1 + c_1(x_2 - x_4)) \\ &= tanh(\Gamma x) \end{aligned} \tag{13}$$

where $\Gamma = \begin{bmatrix} k_1, & c_1, & 0, & -c_1, & 0 \end{bmatrix}$

Therefore, $\Phi(x, u)$ satisfies the Lipschitz condition in x

$$\|\Phi(x) - \Phi(\hat{x})\| \leqslant \|\Gamma(x - \hat{x})\|, \forall x, \hat{x} \tag{14}$$

From (6) and Remark 3, the estimation error dynamics of $\mathcal{H}_\infty$ Lipschitz observer is obtained

$$\begin{cases} \dot{e} &= (A - L_{\infty L}C)e + B(\Phi(x) - \Phi(\hat{x})) \cdot u \\ &\quad +(D_1 - L_{\infty L}D_2)\omega \\ e_z &= C_z e \end{cases} \tag{15}$$

Assuming the Lipschitz condition (14) for $\Phi(x)$, the $\mathcal{H}_\infty$ Lipschitz observer design objective is stated below

- The system (15) is stable for $\omega(t) = 0$
- $\|e_z(t)\|_{\mathcal{L}_2} < \gamma_{\infty L}\|\omega(t)\|_{\mathcal{L}_2}$ for $\omega(t) \neq 0$

The following theorem solves the above problem into an LMI framwork [10].

Theorem 3 Consider the system model (3) and the observer (4) . The system (15) is asymptotically stable for $\omega = 0$ and $\frac{\|e_z(t)\|_{\mathcal{L}_2}}{\|\omega(t)\|_{\mathcal{L}_2}} < \gamma_{\infty L}$ for $\omega(t) \neq 0$ if there exist a symmetric positive definite matrix $P_{\infty L}$ and a matrix $Y_{\infty L}$ minimizing $\gamma_{\infty L}$ such that:

$$\begin{bmatrix} \Omega & P_{\infty L}B & P_{\infty L}D_1 + Y_{\infty L}D_2 \\ * & -\epsilon_l I_d & 0_{n,d} \\ * & * & -\gamma_{\infty L}^2 I \end{bmatrix} < 0 \tag{16}$$

where $\Omega = A^TP_{\infty L} + P_{\infty L}A - Y_{\infty L}C - C^TY_{\infty L}^T + \epsilon_l\Gamma^T\Gamma + C_F^TC_F$

The corresposding observer gain is given by

$L_{\infty L} = P_{\infty L}^{-1}Y_\infty$

4 Analysis of the observer design: frequency and time domain simulations

In this section, the synthesis results of the $\mathcal{H}_2$, $\mathcal{H}_\infty$ and $\mathcal{H}_\infty$ Lipschitz observers are presented and some simulation results are provided.

4.1 Synthesis results and frequency domain analysis

Solving theorem 1, theorem 2 and theorem 3 leads the following solutions: the gains $\gamma_2 = 3.1917$, $\gamma_\infty = 1.4142$, $\gamma_{\infty L} = 1.0032$, $\epsilon_l = 2.0010$ and the observer gains

$$L_2 = \begin{bmatrix} -0.36446 & 0.0069 \\ -0.0102 & 0.0187 \\ 9.1060 & -104.3039 \\ -0.101 & 1.002 \\ -2.2303 \times 10^4 & 0.0441 \times 10^4 \end{bmatrix}$$

$$L_\infty = \begin{bmatrix} -0.0162 & 0.0003 \\ 0.9538 & 0.0007 \\ -5.5702 & -0.0277 \\ -0.0046 & 1.0010 \\ -139.6485 & 5.9865 \end{bmatrix}$$

$$L_{\infty L} = \begin{bmatrix} -32.4356 & 0.0289 \\ -23.9485 & 0.0221 \\ -4.7906 & -8.8192 \\ -2.4948 & 1.0022 \\ -1.6787 \times 10^4 & 15.2625 \end{bmatrix}$$

The resulting attenuation of the sensor noises and derivative road profile disturbance on the estimation error are illustrated in Figures 2 and 3. These figures emphasize the attenuation level of the measurement noises and unknown road profile effect on the 4 estimation errors. The largest sensor noise and derivative road profile disturbance amplication of the 4 errors, over the whole frequency range ($[1, 10^7]$ Hz for sensor noise and $[0.1, 10^8]$ Hz for derivative road profile disturbance), are -13dB at 1 Hz and -17.6dB at 0.1 Hz, respectively.

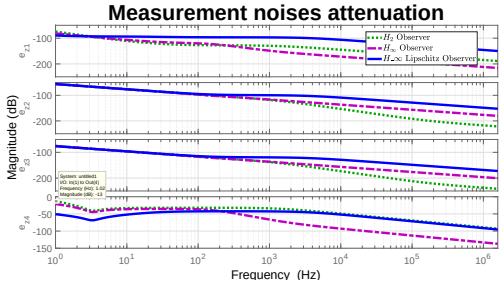

Figure 2. Measurement noises attenuation

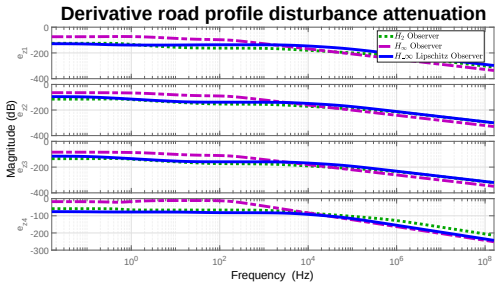

Figure 3. Derivative road profile disturbance attenuation

4.2 Simulation

To evaluate the effectiveness of the proposed algorithms, the following simulations are carried out with the initial conditions of the observers states: $\hat{x}_0 = \begin{bmatrix} 0.01, & 0.1, & 0.001, & 0.1, & 4 \end{bmatrix}^T$ and 0 for the simulated system.

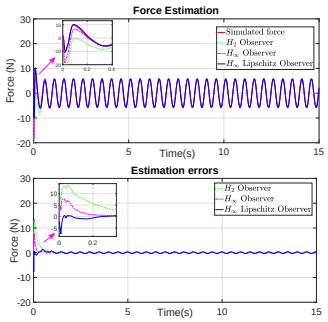

Figure 4. Simulation results: Estimated force and estimation errors

The following simulation scenario is considered to compare the performance of the proposed observers:

- Road profile: The sequence of sinusoidal bumps (2Hz)
- The control input u is constant ($u = 0.2$)

5 Experimental validation

To experimentally assess and compare the effectiveness of the proposed methodologies, the proposed observers are implemented on the 1/5 car scaled car INOVE available at GIPSA-lab, shown in Fig. 5.

This test-bench is equipped with 4 semi-active ER suspensions, which is controlled in real-time using Matlab real-time workshop and a host computer. The three observer system is implemented with the sampling period $T_s = 0.005s$. Note that the experimental platform is fully equipped with sensors to measure its vertical motion. At each corner of the system, a DC motor is used to generate the road profile.

The observers are applied on the rear-left corner using two accelerometers: the unsprung mass $\ddot{z}_{us}$ and the sprung mass $\ddot{z}_s$. For validation purpose only, the damper force

sensor is used to compare the measured force with the estimated one. The following block-scheme illustrates the experimental scenario of the observer (shown in Fig. 6)

Figure 5. The experimental testbed INOVE at GIPSA-lab (see www.gipsa-lab.fr/projet/inove)

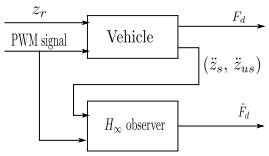

Figure 6. Block diagram for the implementation of the observers

The experimental scenario is as follows

- The road profile is a sequence of sinusoidal bumps
- The control input u is constant ($u = 0.2$)

The experiment results of the observer are presented in Fig. 7. The result illustrates the accuracy and effciency of the proposed observers. To further describe this accuracy, Table 1 shows the normalized root-mean square errors, considering the difference between the estimated and measured forces in the experiment tests

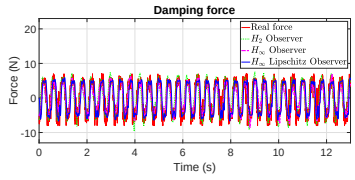

Figure 7. Experimental results: Estimated force

Table 1. Normalized Root-Mean-Square Errors (NRMSE)

Observer	NRMSE
H_2 Observer	0.1104
H_∞ Observer	0.1032
H_∞ Lipschitz Observer	0.0896

6 Conclusion

This paper developed and compared several observers to estimate the damper force, using a dynamic nonlinear model of the ER damper. For this purpose, the quarter-car system is represented in state-space form by considering a phenomenological model of the damper. Based on two accelerometers, the observers are designed, giving a good estimation result of the damping force. The estimation error is minimized, accounting for the effect of unknown inputs (road profile disturbance and measurement noises) and the nonlinearity term bounded by a Lipchitz condition. Both simulation and experiment results assess the ability and the accuracy of the proposed models to estimate the damping force of the ER semi-active damper.

References

[1] S.M. Savaresi, C. Poussot-Vassal, C. Spelta, O. Sename, L. Dugard, *Semi-active suspension control design for vehicles* (Elsevier, 2010)

[2] C. Poussot-Vassal, C. Spelta, O. Sename, S.M. Savaresi, L. Dugard, Annual Reviews in Control **36**, 148 (2012)

[3] C. Poussot-Vassal, O. Sename, L. Dugard, P. Gaspar, Z. Szabo, J. Bokor, Control Engineering Practice **16**, 1519 (2008)

[4] G. Priyandoko, M. Mailah, H. Jamaluddin, Mechanical systems and signal processing **23**, 855 (2009)

[5] G. Koch, T. Kloiber, B. Lohmann, in *Decision and Control (CDC), 2010 49th IEEE Conference on* (IEEE, 2010), pp. 5592–5597

[6] A.Estrada-Vela, D.H. Alcántara, R.M. Menendez, O. Sename, L. Dugard, IFAC-PapersOnLine **51**, 764 (2018)

[7] J.C. Tudon-Martinez, D. Hernandez-Alcantara, O. Sename, R. Morales-Menendez, J.d.J. Lozoya-Santos, IFAC-PapersOnLine **51**, 19 (2018)

[8] R. Rajamani, J.K. Hedrick, IEEE Transactions on control systems technology **3**, 86 (1995)

[9] M. Reichhartinger, R. Falkensteiner, M. Horn, IFAC-PapersOnLine **51**, 328 (2018)

[10] T.P. Pham, O. Sename, L. Dugard, in *9th IFAC International Symposium on Advances in Automotive Control (AAC 2019)* Orléans, France, 2019

[11] C. Scherer, S. Weiland, Lecture Notes, Dutch Institute for Systems and Control, Delft, The Netherlands **3** (2000)